

Spectroscopy and Photochemistry of Ketene Adsorbed to Sodium Chloride

Otto Berg and George E. Ewing*

Department of Chemistry, Indiana University, Bloomington, Indiana 47405 (Received: November 27, 1990)

Infrared and ultraviolet absorption spectroscopies are used to investigate the photochemistry of ketene (CH_2CO) adsorbed to a film of NaCl crystallites. The vibrational spectrum of adsorbed ketene resembles that of condensed and matrix-isolated samples: transition frequencies and intensities are only slightly modified. The electronic spectrum, however, shows significant shifts and enhancements due to adsorption. Following 185-nm excitation, adsorbed ketene dissociates with near unit efficiency. Secondary reaction of methylene radicals (CH_2) is complete, producing ethylene (C_2H_4) and carbon monoxide (CO). For 254-nm excitation the quantum yield of dissociation is $<10^{-2}$, significantly lower than in the gas. Quenching mechanisms are discussed in light of the known dynamical properties of ketene molecules and NaCl crystals.

The development of matrix isolation is one of George C. Pimentel's prime research achievements. In 1954 his seminal publication with Whittle and Dows proposed a method to trap active molecules in a solid matrix of inert material.¹ Hundreds of subsequent papers (reviewed in refs 2-5) attest to the remarkable success of this technique, principally for the study of reactive species. In addition, matrix isolation has proved valuable for the investigation of molecular motion and interaction in the condensed phase,^{6,7} conformational isomerism,⁸ and energy transfer.⁹ Here we will show that porous films of alkali-metal halides, as substrates for molecular adsorption, mimic and complement the spectroscopic utility of frozen matrices.

The isolating medium in question is the large surface area of a sublimed alkali-metal halide film (NaCl, KBr, LiF, etc.). The film consists of loosely packed crystallites of the salt. Molecules to be studied are held by electrostatic attraction to the surface of these crystallites. Like the frozen rare gases that serve as the matrix isolation environment, alkali-metal halide films are optically transparent throughout the infrared, visible, and near-ultraviolet frequencies. Since alkali-metal and halide ions have closed electronic shells, their configurations resemble the corresponding rare gas. The surface of such a film is often chemically inert to adsorbed molecules.

Alkali-metal halides were first exploited as substrates for electronic absorption spectroscopy over 50 years ago by de Boer.¹⁰ They were rediscovered decades later by Kozirovsky and Folman,¹¹⁻¹³ who developed their potential for infrared spectroscopy of small adsorbed molecules. From time to time others have used alkali-metal halide films as substrates for molecular spectroscopy.¹⁴⁻¹⁶ Heidberg and Hussla¹⁵ have already noted interesting analogies between matrix isolation and alkali-metal halide film spectroscopy. In an infrared spectroscopic study, Edling, Richardson, and Ewing¹⁷ demonstrated the close connection between NaCl film and solidified rare gas as trapping environments for

methane. Kirkor, David, and Michl have investigated the photochemistry of molecules permanently incorporated within alkali-metal halides.¹⁸

This paper explores the spectroscopic and photochemical behavior of ketene (CH_2CO) adsorbed to a sodium chloride film. The choice of ketene for our study provides an interesting comparison with extensive gas-phase and matrix isolation studies of this system.¹⁹⁻²¹ In all cases, the primary products of near-ultraviolet photolysis of ketene are carbon monoxide (CO) and methylene radical (CH_2). We will show that, as in matrix studies, the internal vibrational frequencies are little affected by molecular physisorption. On the other hand, whereas an inert gas cage prevents separation of photofragments,^{19,20,22,23} products of ketene photolysis are easily detected in the salt film. Significant modification of the gas-phase electronic absorption spectrum and photodissociation yield will also be documented. These effects will be compared to recent studies of molecular photodissociation on LiF single crystals.²⁴ Detailed theoretical^{25,26} and experimental^{27,28} studies of gas-phase ketene by other researchers are instrumental to our analysis.

Equipment and Procedures

NaCl Films. The substrate for adsorption was prepared and characterized according to techniques described by Richardson et al.²⁹ Figure 1 is a schematic cross section of the film photochemistry apparatus. The brass sample cell was mounted to a cryostat whose temperature could be actively controlled from 20 to 300 K. A stainless steel tube connected the interior of the sample cell to a vacuum manifold. Here equilibrium vapor pressures and the pressures of gas doses were measured with a capacitance manometer. The temperature controller was calibrated with respect to vapor pressures of pure substances condensed in the cell.

All spectra presented here were recorded in the film cell. Barium fluoride was chosen as a window material because it is transparent throughout the mid-infrared and near-ultraviolet regions. The windows were sealed to the cell with indium gaskets.

(1) Whittle, E.; Dows, D. A.; Pimentel, G. C. *J. Chem. Phys.* **1954**, *22*, 1943.

(2) Cradock, S.; Hinchcliffe, A. J. *Matrix Isolation*; Cambridge University Press: Cambridge, 1975.

(3) Weltner, W. Jr. *Adv. High Temp. Chem.* **1969**, *2*, 85.

(4) Andrews, L. *Annu. Rev. Phys. Chem.* **1979**, *30*, 79.

(5) Andrews, L.; Moskovits, Eds. *Chemistry and Physics of Matrix Isolated Species*; Elsevier: Amsterdam, 1989.

(6) Pimentel, G. C.; Charles, S. W. *Pure Appl. Chem.* **1963**, *7*, 111.

(7) Frayer, F. H.; Ewing, G. E. *J. Chem. Phys.* **1968**, *48*, 781.

(8) Frei, H.; Pimentel, G. C. *Annu. Rev. Phys. Chem.* **1985**, *36*, 491.

(9) Bondybe, V. E. *Annu. Rev. Phys. Chem.* **1984**, *35*, 591.

(10) de Boer, J. H. *Electron Emission and Adsorption Phenomena*; Cambridge University Press: Cambridge, 1935.

(11) Kozirovski, Y.; Folman, M. *J. Chem. Phys.* **1964**, *41*, 1509.

(12) Kozirovski, Y.; Folman, M. *Trans. Faraday Soc.* **1966**, *62*, 808.

(13) Gevirzmann, R.; Kozirovski, Y.; Folman, M. *Trans. Faraday Soc.* **1969**, *65*, 2206.

(14) Hartmann, H.; Luchterhand, H. *Z. Phys. Chem. (Munich)* **1965**, *46*, 103.

(15) Heidberg, J.; Hussla, I.; in Caudano, R.; Gilles, J.-M.; Lucas, A. A. *Vibrations at Surfaces*; Plenum Press: New York, 1982; p 323.

(16) Smart, R. St. C.; Sheppard, N. *J. Chem. Soc., Faraday Trans. 2* **1976**, *72*, 707.

(17) Edling, J. A.; Richardson, H. H.; Ewing, G. E. *J. Mol. Struct.* **1987**, *157*, 167.

(18) Kirkor, E. S.; David, D. E.; Michl, J. *J. Am. Chem. Soc.* **1990**, *112*, 139.

(19) DeMore, W. B. Doctoral Dissertation, California Institute of Technology, 1958.

(20) Milligan, D. E. Doctoral Dissertation, University of California, Berkeley, 1958.

(21) Moore, C. B.; Pimentel, G. C. *J. Chem. Phys.* **1963**, *38*, 2816.

(22) Jacox, M. Private communication.

(23) Moore, C. B.; Pimentel, G. C. *J. Chem. Phys.* **1964**, *41*, 3504.

(24) Leggett, K.; Polanyi, J. C.; Young, P. A. *J. Chem. Phys.* **1990**, *93*, 3645 and references cited therein.

(25) Dykstra, C. E.; Schaefer III, H. F. *J. Am. Chem. Soc.* **1976**, *98*, 2689.

(26) Allen, W. D.; Schaefer III, H. F. *J. Chem. Phys.* **1988**, *89*, 329 and references cited therein.

(27) Chen, I.-C.; Green, Jr., W. H.; Moore, C. B. *J. Chem. Phys.* **1988**, *89*, 314.

(28) Potter, E. D.; Gruebele, M.; Khundkar, L. R.; Zewail, A. H. *Chem. Phys. Lett.* **1989**, *164*, 463.

(29) Richardson, H. H.; Baumann, C.; Ewing, G. E. *Surf. Sci.* **1987**, *185*, 15.

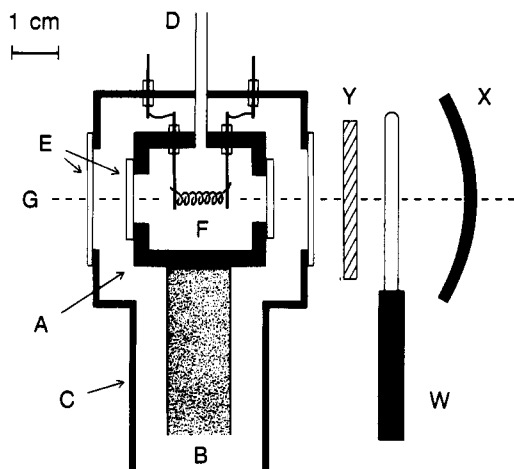


Figure 1. Apparatus for NaCl film experiments: (A) sample cell; (B) cryostat; (C) insulating shroud; (D) connection to vacuum manifold; (E) BaF₂ windows; (F) sublimation filament; (G) ultraviolet and infrared optical axis; (W) Hg discharge lamp; (X) spherical mirror; (Y) glass filter.

Their limiting aperture was 1.1 cm, and they were separated by an inner path length of 3.85 cm. The optical axis was horizontal, and the cell was small enough to fit in the sample compartments of our infrared and ultraviolet spectrophotometers.

A 2 mm × 10 mm helical tungsten filament was mounted in the center of the cell. Before each run a crystal of NaCl weighing 10–50 mg was placed within this filament. In order to deposit a film, the cell was evacuated and cooled to 77 K and then the filament brought to an orange glow. The salt was allowed to sublime for 12–24 h. When the crystal was significantly or entirely consumed the filament was turned off. The film was treated for increased porosity by twice condensing a visible amount of N₂ in the cell and then pumping the liquid away. Finally the film was subjected to at least one annealing cycle: approximately 20 mbar of N₂ was sealed into the cell, it was warmed to 250 K, then cooled to 83 K, and characterized with CO. A film was considered sufficiently annealed when the vibrational bandwidth (fwhm) of CO at $\theta = 0.9$ coverage fell below 10 cm⁻¹.

Volumetric calibration of the film cell and manifold was achieved through systematic expansions and the ideal gas law. The number of molecules in a gas aliquot, and the number adsorbed when such an aliquot was exposed to a film, were calculated accordingly. Isotherms were recorded by successive dosing of a film followed by equilibrium pressure measurements.

Spectroscopy and Photolysis. Vibrational spectra were recorded with a Fourier transform infrared spectrophotometer (Mattson Nova Cygni 120). A room-temperature TGS detector was used, and the nominal resolution was set at 2.0 cm⁻¹. A background was collected for every temperature under investigation. Each background and sample interferogram consisted of 1500 coherently averaged scans. The interferograms were extended with zeros by a factor of 4 and then transformed without an apodization function. Absorbance, $A = \log(I_0/I)$, was plotted as a function of wavenumber $\bar{\nu}$, using a single-beam sample spectrum and the appropriate background. In some cases a computer program was used to calculate the difference between two absorbance spectra. A computer program was also used to integrate absorbance bands. The program fit a linear baseline to specified regions and then calculated the integrated absorbance:

$$\bar{A} = \int_{\text{band}} \log(I_0/I) d\bar{\nu} \quad (1)$$

The interferometer and sample changer were purged with dry nitrogen in order to eliminate atmospheric absorbances.

Infrared absorption spectra were used to monitor the progress of photochemical reactions with time. Figure 1 illustrates the ultraviolet optical elements in their relation to the film cell. The source was a small, low-pressure mercury discharge lamp (Orion Hg(A)). Such lamps radiate primarily through two mercury

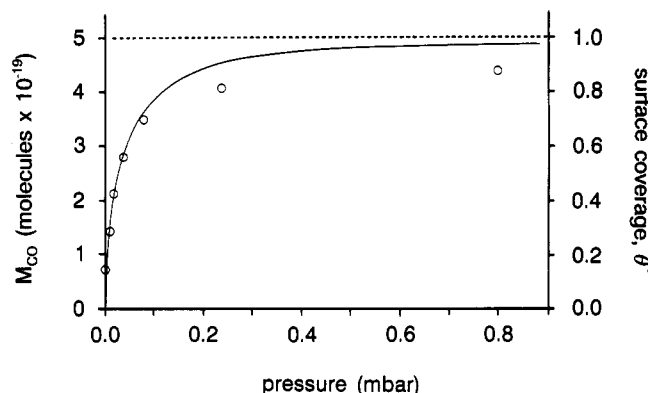


Figure 2. Adsorption isotherm of CO on NaCl film at 83 K. Open circles are data points; the broken line indicates monolayer coverage. The solid line is a Langmuir-type isotherm fit to the data. This film was the substrate for infrared and photochemical studies of adsorbed ketene; it weighed 23 mg.

resonance lines: 185.4 and 253.7 nm.^{30,31} The intensity of the former with respect to the latter is in the range 10–15%.³² The lamp dissipated only ~1.6 W overall; the irradiance of 254-nm light at 1-in. distance was $2.3 \times 10^3 \mu\text{W cm}^{-2}$.³³ An aluminum-coated spherical mirror focused light into the film cell. For some experiments a glass filter (Corion UG-5-S) was placed between the lamp and film cell. The filter was opaque to 185-nm light and most visible and infrared frequencies. It transmitted a broad band of ultraviolet light between 220 and 420 nm; its external transmittance at 254 nm was 55%.³³

Electronic spectra from 400 to 185 nm were recorded with a rugged Cary 14R spectrophotometer. The wavelength scale was calibrated according to the Cameron bands in a sample of CO gas.³⁴ These bands also demonstrated that the instrumental resolution was 1 nm at wavelengths greater than 190 nm. Between 190 and 185 nm the instrumental resolution was degraded by atmospheric absorption. In some cases absorbance features in a baseline spectrum were subtracted from a sample spectrum.

Samples. Ketene was generated by the pyrolysis of acetone in a "reflux lamp" adapted from existing designs.^{35,36} Three traps at 196 K removed unreacted acetone from the product stream; ketene was collected in a final trap at 142 K. Uncondensable gases were removed from the raw product by several freeze/pump/thaw cycles. The product was distilled from a trap at 175 K to one at 142 K, and a narrow middle fraction was retained. This purified product was stored at 77 K in the dark. Its vapor pressure at 175 K was ~40 mbar, as expected for ketene.³⁷ Such vapor was used for all experiments. Infrared spectra of gaseous and adsorbed samples showed trace amounts of CO₂ and C₂H₄.

Results

Characterization of Films. A large number of NaCl films have been prepared in our laboratory; their properties can be rather closely controlled.^{17,29} Following deposition and annealing, films are typically visible as a faint fogging of the cell windows. Under certain lighting conditions thin film interference fringes can also be seen. Familiarity with the adsorption of CO on various films allows us to use its thermodynamic and spectroscopic properties as diagnostic tools.

(30) Calvert, J. G.; Pitts, J. N., Jr. *Photochemistry*; John Wiley & Sons: New York, 1966.

(31) Okabe, H. *Photochemistry of Small Molecules*; John Wiley & Sons: New York, 1978.

(32) Beckey, Von H. D.; Groth, W.; Okabe, H.; Rommel, H. *J. Z. Naturforsch.* **1964**, *A19*, 1511.

(33) Orion catalog, Corion catalog.

(34) Herzberg, G. *Molecular Spectra and Molecular Structure*; Van Nostrand Reinhold: New York, 1950; Vol. I.

(35) Williams, J. W.; Hurd, C. D. *J. Org. Chem.* **1940**, *5*, 122.

(36) Dunbar, R. E.; Bolstand, L. J. *J. Org. Chem.* **1944**, *9*, 219.

(37) Reuben, J. *Chem. Eng. Data* **1969**, *14*, 235.

(38) Steele, W. A. *The Interaction of Gases with Solid Surfaces*; Pergamon: Oxford, 1974.

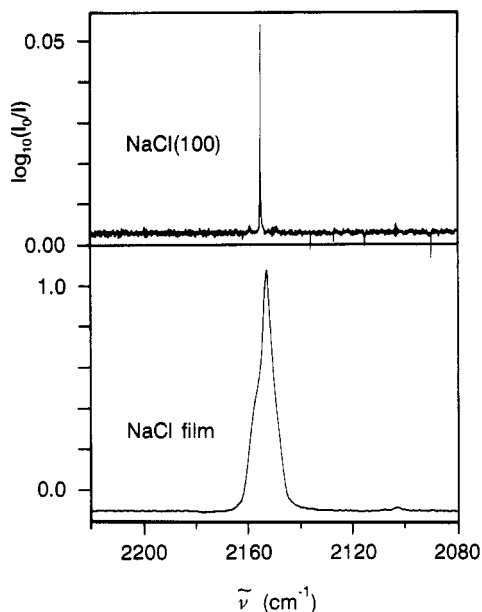


Figure 3. Comparison of the infrared spectra of CO adsorbed to NaCl(100) single crystal (upper spectrum)³⁹ and CO adsorbed to an annealed NaCl film (lower spectrum). Both represent monolayer coverage at 30 K.

An adsorption isotherm for CO at 83 K is plotted in Figure 2. (This particular film, resulting from a 23-mg deposit, was the substrate for the infrared and photochemical experiments discussed here. Another film was used for ultraviolet absorption measurements.) The number of CO molecules adsorbed is plotted against the equilibrium pressure. Adsorption is a reversible process: reducing the equilibrium pressure reduces the number of CO molecules on the surface.²⁹ Beyond 5 mbar no further adsorption of CO can be detected, therefore the film is saturated. As indicated by the broken line, this coverage corresponds to a monolayer of CO. The coverage relative to this limit is given by the parameter θ .

Spectroscopy of CO on NaCl crystallites has been the subject of numerous investigations.^{13,15,29} We reproduce a typical spectrum for $\theta = 1.0$ at 30 K in Figure 3. This spectrum is compared to $\theta = 1.0$ for CO on the (100) face of a single NaCl crystal, also at 30 K. The central absorption features on both the single crystal (2155.1 cm^{-1}) and the annealed film (2152.2 cm^{-1}) are close in frequency. However, CO bandwidths (fwhm) differ considerably: 0.25 cm^{-1} on the single crystal, 8.0 cm^{-1} on the film. Moreover, a distinct shoulder appears in the film spectrum near 2158 cm^{-1} . Spectra of CO adsorbed to unannealed films show additional features and more diffuse profiles.²⁹

Infrared Spectra. In order to minimize the thermally initiated reactions, it was desirable to adsorb ketene at the lowest possible temperature. Sufficient thermal energy was necessary, however, to allow diffusion into the film and to avoid bulk condensation. At 150 K the vapor pressure of bulk ketene is ~ 4 mbar;³⁷ all ketene dosing was performed at this temperature, with aliquot pressures of 2 mbar or less.

Infrared spectra of ketene adsorbed to the film characterized in Figure 2 are shown in Figure 4, at $\theta_r = 0.14$ and $\theta_r = 0.55$. The subscript r on θ indicates that these coverages are relative to a monolayer of CO. We wish to distinguish experimentally between the following classes of signals: those due to ketene, to contaminants in the ketene sample, and to products of reaction among adsorbed molecules. Signals of the second kind are identified by independent spectroscopic characterization of the appropriate species. Signals of the first and third kind are separated by promoting reaction and monitoring its effect on the spectrum. To this end, a film dosed with ketene at 150 K was warmed to 210 K and returned to 150 K. This operation depleted the signals that are most prominent in Figure 4: all absorbances between 3300 and 2900 cm^{-1} ; the strong feature at 2124 cm^{-1} ; signals at 1930, 1379, 1133, and 971 cm^{-1} . The temperature cycle enhanced some

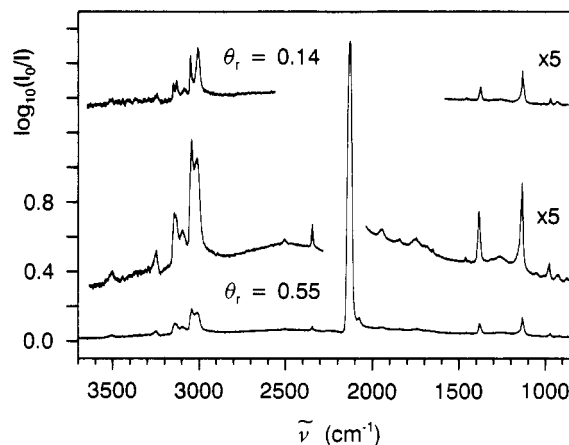


Figure 4. Infrared spectra of ketene adsorbed to NaCl film at 150 K. Coverage values are relative to a CO monolayer. Fundamental vibrations of ketene are identified in Table I; impurities are discussed in the text.

of the weak bands found in Figure 4: all absorbances between 1900 and 1600 cm^{-1} ; signals at 1245, 1040, and 865 cm^{-1} . Similarly, dosing a film to $\theta_r > \sim 0.5$ increased the intensity of the latter group of signals relative to the former. The effects of photochemical reaction are described separately below. Since the latter group of absorbances is evidently not due to ketene, we concentrate now on the former.

The spectra in Figure 4 were recorded after the first and last of four approximately equal aliquots. The integrated areas of the bands at 2124, 1379, and 1133 cm^{-1} increase linearly with coverage in this range. We will later use these areas to calculate empirical integrated cross sections for the corresponding molecular vibrations. The total area of the absorbances between 3200 and 2900 cm^{-1} also increases linearly with coverage. However, this is not true of the individual components. Two doublets are observed, 3150/3130 and 3049/3006 cm^{-1} , which overlap with a single peak at 3090 cm^{-1} . At very low coverage ($\theta_r = \sim 0.05$, not shown) only the low-frequency component of each doublet is present. With increasing coverage, growth of the high-frequency components is favored (Figure 4). The spectra are too congested to allow integration of these peaks individually. It is not clear whether the low-frequency components reach a saturated intensity.

These infrared signals cannot be removed by pumping on the film. With increasing temperature, conversion of the first group of absorbances to the second proceeds without a significant increase in vapor pressure. Therefore, the NaCl films can only be dosed additively, and thermodynamic characterization of this system is not possible.

Ultraviolet Spectra. The empty film cell had an ultraviolet absorbance (due to the BaF_2 windows) which increased with decreasing wavelength. Absorbance at 254 and 185 nm was 0.08 and 0.28, respectively. This signal was removed by the use of a reference blank. Gaseous ketene at room temperature was then allowed into the cell. Spectra were recorded at two pressures, 28 and 1.3 mbar. These are shown in Figure 5 (broken lines). The cell was then evacuated and cooled for NaCl sublimation.

Following the film deposit, a uniform increase in the baseline of $A = 0.04$ was observed from 400 to 220 nm. Absorbance increased sharply at wavelengths less than 220 nm, reaching 0.38 at 185 nm. After one annealing cycle the film had a uniform 0.38 ± 0.12 absorbance at 400 to 185 nm ($\sim 60\%$ of light intensity lost). This was flattened and set to zero electronically.

The film was dosed with ketene at 150 K. Adsorbed phase spectra are shown in Figure 5 (solid lines). Three regions of diffuse absorption are apparent. For $\theta_r = 0.57$ two bands are centered at 265 and 330 nm. These are shifted to shorter wavelength—250 and 300 nm—at $\theta_r = 0.13$ (not shown in Figure 5). The third signal peaks below 200 nm at $\theta_r = 0.13$; the cell is opaque below 215 nm for $\theta_r = 0.57$ ($A > 2$). This signal embraces the strong gas-phase progression at 213 nm. There is a similar correspondence between the long-wavelength absorption (300–350 nm) of the adsorbed and gaseous phases. However, the adsorbed-phase

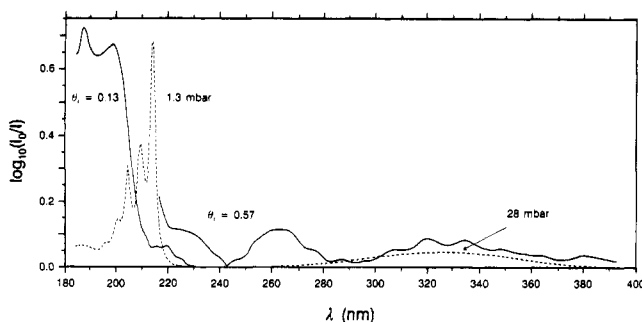


Figure 5. Ultraviolet spectra of ketene gas at room temperature (broken lines) and ketene adsorbed to NaCl film at 150 K (solid lines). Coverage values are relative to a CO monolayer.

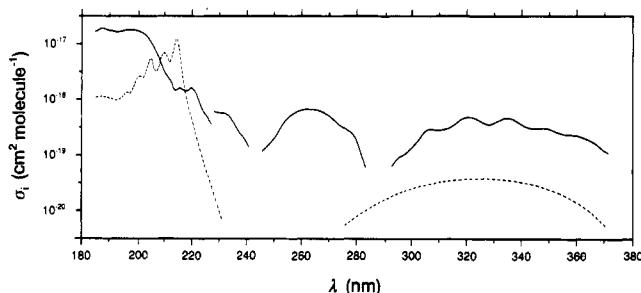


Figure 6. Molecular ultraviolet cross sections for ketene gas at room temperature (broken lines) and ketene adsorbed to NaCl film at 150 K (solid lines).

signal near 265 nm has no parallel in the gas.

Cycling a dosed film to 210 K or dosing it to $\theta_r > 0.5$ had the same effect: the structure described above was replaced by smooth, strong absorbance. This signal began at ~ 320 nm and increased monotonically toward shorter wavelength; the cell typically became opaque at 220 nm.

Photolysis of Adsorbed Ketene. After the film characterized in Figure 2 had been dosed to $\theta_r = 0.55$, the cell was cooled to 20 K. At this temperature the film was alternately irradiated with ultraviolet light and interrogated by infrared absorption spectroscopy. The initial photolysis period was 5.5 h, during which the glass filter was in place; only 254-nm light entered the cell. After this the filter was removed, allowing both 254- and 184-nm light to pass. The film was irradiated for four 15-min periods, followed by a 1-h exposure.

This procedure depleted all of the infrared absorption signals found in Figure 4 except three: the integrated areas of peaks at 2345, 1444, and 971 cm^{-1} increased. In addition, the peak at 2124 cm^{-1} developed a high-frequency shoulder while being depleted overall. Figures 7 and 8 present pairs of spectra which illustrate these effects. The lower traces were recorded prior to any irradiation. The sample was therefore identical with that in Figure 4, $\theta_r = 0.55$, but cooled to 20 K. The upper traces were recorded after the final ultraviolet exposure.

The high-frequency portion of Figure 7 shows that this congested region is depleted uniformly; coverage dependence of relative intensities in the doublets is *not* observed during photochemical consumption. The low-frequency portion shows the growth of a product band at 1444 cm^{-1} , as well as uniform loss of intensity at 1379 cm^{-1} . Figure 8 presents "before" and "after" spectra of the 2124-cm^{-1} signal, which is not depleted uniformly; a shoulder appears at 2153 cm^{-1} . It is another product peak, which can be separated from the broad central feature by scaling bandshape b and subtracting it from a. The result is given in Figure 8 and described below.

Discussion

NaCl Surface. Characterizing the substrate by CO absorption serves three functions. First, it relates the present work to previous studies of related systems, thereby providing morphological information not directly available from our data. Second, it allows quantitative comparison between experiments performed on

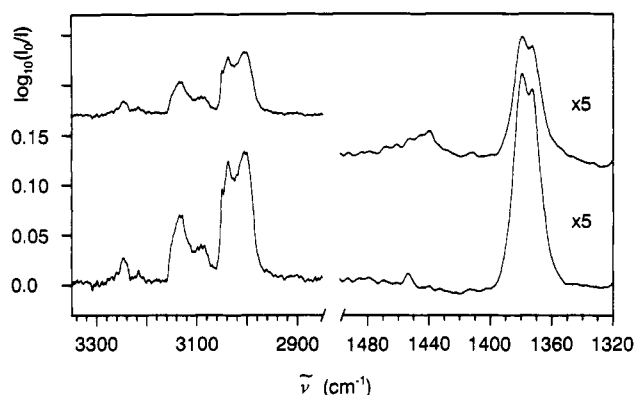


Figure 7. Infrared spectra of adsorbed ketene at 20 K before (lower trace) and after (upper trace) exposure to 185-nm light. Uniform loss of signals due to ketene is accompanied by growth of a signal due to ethylene.

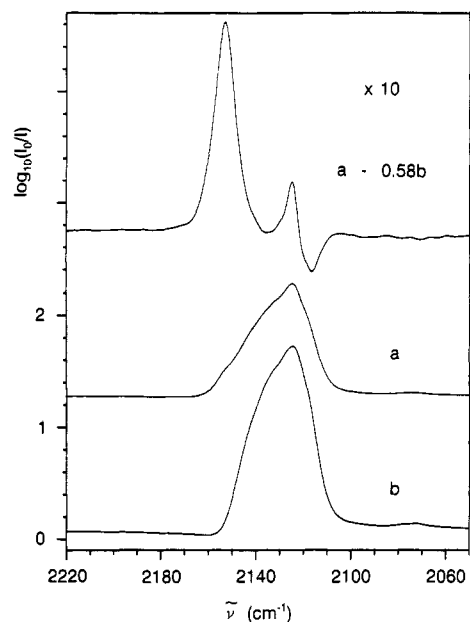


Figure 8. Infrared spectra of adsorbed ketene at 20 K before (b) and after (a) exposure to 185-nm light. The shoulder that appears in (a) is due to CO. In the upper trace this signal is reconstructed by scaling (b) and subtracting it from (a), as described in the text.

different films. This is particularly important for the present research since an individual film cannot be cleaned following exposure to ketene, yet the various observations that contribute to our physical understanding cannot be made simultaneously. Knowledge of the molecular capacity of a film prior to dosing allows comparable coverages to be reached on separate films. Finally, a model adsorbate can connect different measures of coverage (volumetric and photometric) that are based in different samplings of the same surface.

It is argued elsewhere¹³ that CO adsorbs to Na^+ sites on the surface of the salt. Thus, the number of CO molecules that saturate the salt film equals the total number of Na^+ ions on the surface of the crystallites. Moreover, electron microscopy reveals that the crystallites are nearly perfect cubes, structurally similar to bulk crystal with exposed (100) faces. The number of CO molecules adsorbed at $\theta = 1$ together with the mass of NaCl sublimed can be used to calculate the number of Na^+ sites per gram. With the known density of bulk NaCl this determines a typical dimension for crystallites in the film. The limiting coverage of the film in Figure 2, 5.0×10^{19} CO molecules, corresponds to cubic crystallites of edge length 8 nm and a total surface area of 8 m^2 .

A Langmuir isotherm is fitted to the data in Figure 2 (solid line). Assuming that adsorption sites are independent and localized, this theoretical model takes the form

$$\theta = \chi(T)p/[1 + \chi(T)p] \quad (2)$$

Here $\chi(T)$ is an equilibrium constant whose value can be empirically determined or calculated from statistical mechanics,²⁹ and p is the equilibrium pressure. The isotherm in Figure 2 was adjusted to match the observed monolayer limit and the equilibrium pressure at $\theta = 0.5$. General agreement with the Langmuir model supports a picture of CO physisorbed to well-separated Na⁺ sites.

That the infrared spectra of CO on microscopic crystallites and bulk single crystals differ as in Figure 3 is consistent with differences in the (100) face expanses available for adsorption. Anomalous sites at steps or edges of small cubes contribute heterogeneously to spectra. The broad features and distinct shoulder in film spectra are explained by CO adsorption to faces of different size, steps, and edges. The featureless and narrow absorption of CO on single-crystal NaCl, by contrast, reflects the virtual absence of defects on the (100) face.

The ultraviolet absorption of NaCl films has been the subject of previous studies.^{10,39} Diffuse absorption features have been assigned to color centers created by the sublimation process. The highest energy signals (278 and 235 nm) are attributed to cation vacancies (V_1 and V_2 centers). The uniform absorbance of $A = 0.38$ in our annealed film must be an ill-defined combination of absorption by color centers and surface defects and light losses due to interference effects and interface reflections.

The sublimation process deposits NaCl on most inner surfaces of the cryogenic cell. Measurements of adsorbate/vapor equilibrium as in Figure 2 reflect the behavior of this entire film. Spectroscopic measurements, on the other hand, only sample that portion of the film which is deposited on the cell windows. In order to couple photometric and volumetric observations, it is necessary to know what fraction of the film is spectroscopically visible. On geometric grounds (see Figure 1) we expect $\sim 4\%$ of the film to condense on the windows. Alternatively, the empirical infrared cross section for adsorbed CO²⁹ indicates that 3.2% of a gaseous aliquot ends up in the infrared beam. We prefer the latter measure with a generous error range, $3.2 \pm 0.8\%$.

Finally, we remark on cleanliness. The vacuum system alone is insufficient to maintain an atomically clean surface. This is achieved instead by the unusual nature of vapor-deposited films. The number of adsorption sites in the film of Figure 2, for example, corresponds to ~ 8 m² of NaCl surface. This is created suddenly, under vacuum, and in a closed and convoluted form—the external surface of the film is small by comparison. Contamination is limited by the mass-transfer rate of irremovable molecules (mainly H₂O), which must diffuse through the vacuum line and the tortuous bulk of the film. In the worst case, significant contamination by ambient gases requires several days to develop. Similarly, gas pressure within the body of the film does not reflect the base pressure of the vacuum line. It is determined, rather, by adsorption equilibria of the molecules present. At 20 K the vapor pressures of all likely adsorbates (except H₂) are vanishingly small. This behavior of the films is analogous to the action of a getter material or sorption pump; under ordinary vacuum pressures, a clean surface is achieved by exploiting the adsorption equilibrium of a vast collection of sites.

Vibrational Assignments. Ketene samples are known to dimerize readily at room temperature. It is expected that the changes observed upon warming on adsorbed sample result from the consumption of ketene and the production of diketene. Indeed, the weak signals in Figure 4 that grow in at high coverage or temperature (1900–1600, 1245, 1040, 865 cm⁻¹) correspond to strong absorbances in the spectrum of gaseous and liquid diketene.⁴⁰

The features that are depleted by a temperature cycle are assigned to ketene. Fundamental vibrational frequencies of adsorbed ketene are listed in Table I together with gas-phase, solid-phase, and argon matrix values. For symmetry labels we adopt

TABLE I: Fundamental Frequency Assignments for Ketene (in cm⁻¹)

mode	gas ^a	matrix ^b	solid ^{b,c}	NaCl film ^d
$\nu_1(a_1)$	3070.5	3062	3043	{ 3049 3006
$\nu_2(a_1)$	151.8	2142	2133	2124
$\nu_3(a_1)$	1388	1381	1374	1379
$\nu_4(a_1)$	1117.8	1115	1131	1133
$\nu_5(b_2)$	3166.1	3155	3140	{ 3150 3130
$\nu_6(b_2)$	976.7	974	975	971
$\nu_7(b_2)$		438	440	
			435	
$\nu_8(b_1)$	588	591	616	
$\nu_9(b_1)$	528	525	529	
			512	

^a Herzberg, G. *Molecular Spectra and Molecular Structure*; Van Nostrand Reinhold: New York, 1966; Vol. III. ^b Moore, C. B.; Pimentel, G. C. *J. Chem. Phys.* **1963**, *38*, 2816. ^c Cox, A. P.; Esbitt, A. S. *J. Chem. Phys.* **1963**, *38*, 1636. ^d This work; $\theta_i = 0.55$ (see Figure 4).

modern convention which locates the x axis normal to the molecular plane^{25,26,41} instead of the y axis, which was used by Moore and Pimentel.²¹ All of the totally symmetric (a_1) vibrations are identified in all phases. Due to the long-wavelength cutoff of the film cell windows, the out-of-plane vibrations (b_1) are not observed. Two of the three in-plane (b_2) vibrations are observed. These frequencies are within 1% of their gas-phase values, while matrix frequencies are even closer. Relative intensities among the six adsorbed-phase features are comparable to both the solid and matrix isolation spectra, with the carbonyl stretch (ν_2) as the dominant absorption.

Absorbance doublets are found in the adsorbed-phase spectrum but not in the solid or matrix. This is most evident in the C–H stretching signals (ν_1, ν_5), for which a coverage-dependent intensity ratio is also observed. Other absorbance bands have structure that is either ill-resolved (ν_2 , Figure 8b), only evident at low temperature (ν_3 , Figure 7), or only evident at lower coverages than those shown here (ν_4). Since we have not investigated the structure of a ketene monolayer, we can only speculate on the origin of these features. They could have the same cause as the shoulder in a CO spectrum (Figure 2): anomalous adsorption sites. Alternatively, crowding at higher coverages may force adsorbed molecules to interact. In either case it is significant that a thermal sampling of different “sites” partitions the molecules among them in a coverage-dependent way (Figure 4). That no such shifting partition is evident during photochemical depletion (Figure 7) shows that the irradiated sample is immobile.

Three unassigned weak signals (3510, 3250, and 3090 cm⁻¹) are depleted in tandem with ketene fundamentals during thermal or photochemical reaction. They are probably combination bands of ketene; several have been observed in this frequency range with matrix-isolated samples.²¹ Similarly, the absorbance at 1930 cm⁻¹ corresponds to the first overtone of ν_6 . Another weak signal (2072 cm⁻¹) arises from ¹³C isotopomers of ketene (ν_2) present in natural abundance.

Ethylene (C₂H₄) is a common byproduct of pyrolytic ketene synthesis and ketene photochemistry. Its infrared spectrum on NaCl films has been recorded.⁴² The strongest signal (ν_7) appears at 975 cm⁻¹, which is coincident with the ν_6 mode of ketene. The next most intense absorbance (ν_{12}) appears at 1441 cm⁻¹ and is present in Figure 4. The signal at 2345 cm⁻¹ arises from carbon dioxide (ν_3). Finally, two weak signals have not been identified: 2500 and 920 cm⁻¹.

Without isotherms it is difficult to describe the state of adsorbed samples. Some features of the infrared spectrum closely resemble those of solid ketene. This could be the result of capillary condensation in small pores.³⁸ On the other hand, unusual response to ultraviolet light leads us to believe that all molecules in the sample are intimately coupled to the substrate.

(39) Smart, R. St. C. *Trans. Faraday Soc.* **1971**, *67*, 1183.(40) Durig, J. R.; Willis, J. N., Jr. *Spectrochim. Acta* **1966**, *22*, 1299.(41) Allen, W. D.; Schaefer III, H. F. *J. Chem. Phys.* **1986**, *84*, 2212.

(42) Schinzer, W. Doctoral Dissertation, Indiana University, 1985.

In order to observe and quantify the photochemical generation of CO, its absorbance must be separated from the broad ν_2 signal of ketene. Fortunately, the ketene profiles do not change shape during depletion. Therefore, the initial ketene ν_2 band (Figure 8b) can be reduced by a scale factor γ and subtracted from subsequent bands to yield a CO signal. The scale factor is chosen according to the following criterion: the integrated absorbance of the difference spectrum from 2135 cm^{-1} (the low-frequency limit of CO absorption) to 2090 cm^{-1} (the low-frequency limit of ketene ν_2 absorption) must equal zero. An example of this procedure is shown in Figure 8 with $\gamma = 0.58$. The frequency and bandwidth of the reconstructed signal agree well with the CO absorbance in Figure 3. Slight discrepancies can be attributed to the subtraction procedure, as well as differences in coverage, temperature, and the kinetics of site selection.

We will need optical cross sections (σ_i , $\text{cm}^2 \text{ molecule}^{-1}$) and integrated optical cross sections ($\bar{\sigma}_i$, cm molecule^{-1}) in the discussion to follow. The most convenient form of the Beer-Lambert law for adsorbed samples is

$$I_0/I = \exp(-N_{2D}\sigma_i) \quad (3)$$

Substituting the definition of absorbance leads to an expression for molecular cross section

$$\sigma_i = 2.303A/N_{2D} \quad (4)$$

where N_{2D} (molecules cm^{-2}) is the density of molecules projected onto a plane normal to the direction of light propagation. The number of molecules in the ketene aliquots is known. Furthermore, it is known that 3.2% of each dose is adsorbed to windows with an effective diameter of 1.1 cm; this allows calculation of N_{2D} and hence σ_i . The subscript on σ_i emphasizes that cross-section values are averaged over all molecular orientations. The integrated cross section $\bar{\sigma}_i$ (cm molecule^{-1}) is obtained by integrating eq 4 over wavenumbers and substituting eq 1.

For the infrared spectra of adsorbed CO we take $\bar{\sigma}_i = 1.4 \times 10^{-17} \text{ cm molecule}^{-1}$ from previous work.²⁹ From the data in Figures 2 and 4 we find for ketene $\bar{\sigma}_i(\nu_2) = 1.2 \times 10^{-16}$, $\bar{\sigma}_i(\nu_3) = 2.7 \times 10^{-18}$, and $\bar{\sigma}_i(\nu_4) = 4.6 \times 10^{-18} \text{ cm molecule}^{-1}$.

The infrared cross sections of adsorbed ethylene and CO_2 have not been measured. Because the NaCl substrate is relatively passive, calculated and gas-phase values provide reasonable first estimates: $\bar{\sigma}_i(\nu_{12}) = 1.2 \times 10^{-18} \text{ cm molecule}^{-1}$ for C_2H_4 ⁴³ and $\bar{\sigma}_i(\nu_3) = 1.1 \times 10^{-16} \text{ cm molecule}^{-1}$ for CO_2 .⁴⁴ These numbers will be employed in the discussion of photochemical stoichiometry.

Electronic Assignments. It is desirable to compare the ultraviolet spectra in Figure 5 on a molecular basis. None of the observed absorbance features were limited by the instrumental resolution. Therefore, the Beer-Lambert law can again relate absorbance to molecular cross section. In the more conventional form of eqs 3 and 4, N_{2D} is replaced by Nl , representing gas density N (cm^{-3}) and path length l (cm). The ideal gas law gives N for gaseous samples, and l is 3.85 cm in the film cell. A plot of molecular cross section for gas-phase ketene is found in Figure 6 (broken line).

The broad, weak absorbance at 325 nm in gaseous ketene has been observed by others.^{45,46} Within the precision of our absorbance measurement ($\pm 20\%$) the maximum molecular cross section agrees with previous reports. The set of four diffuse bands at 213 nm is also familiar.^{46,47} The maximum molecular cross section in Figure 6, however, is 3.2 times greater than that given in ref 46.

Equation 4 also allows the optical cross section of adsorbed molecules to be calculated. This is plotted in Figure 6 (solid line).

Figure 9 summarizes theoretical and experimental investigations of the excited electronic states of ketene. Various determinations of vertical excitation energies are shown with their state assignments. Zero energy is defined as the ground 1A_1 state, from which

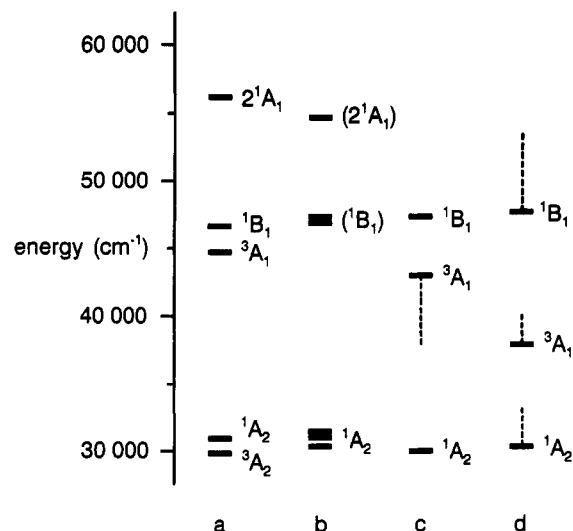


Figure 9. Excited electronic states of ketene. Various state assignments and determinations of vertical transition energy are summarized in four columns: (a) ab initio calculations;⁴¹ (b) ultraviolet absorption measurements;⁴⁵⁻⁴⁸ (c) electron impact energy loss measurements;⁴⁹ (d) adsorbed-phase ultraviolet absorption measurements from this study (Figure 5). Broken lines indicate ranges over which transitions are observed.

these excitations originate. Column a locates the recent ab initio theoretical results of Allen and Schaefer.⁴¹ Schaefer's persistent work on ketene has clarified the available spectroscopic data and highlighted novel aspects of its photophysical behavior. Column b summarizes gas-phase ultraviolet absorption experiments.⁴⁵⁻⁴⁸ Assignments in parentheses are from ref 41. Column c shows results of electron impact energy loss studies.⁴⁹ Since these are not bound by the spin multiplicity selection rule, triplet states have been observed. The broken line on 3A_1 shows the energy range that this signal spans. Column d locates the three absorption regions of ketene on NaCl film. The two low-energy maxima represent $\theta_i = 0.57$; broken lines indicate their observed coverage dependence. Onset of the high-energy signal is also shown, with a broken line indicating its extension to the short-wavelength limit of this experiment.

The adsorbed-phase signal at 330 nm ($30\,000 \text{ cm}^{-1}$) corresponds well to gas-phase excitation of the 1A_2 state. The maximum molecular cross section, however, is 10 times greater in the adsorbed phase. Some enhancement is to be expected because a $^1A_2 \leftarrow ^1A_1$ transition is electric dipole forbidden. It is only by virtue of vibrational symmetry breaking that this transition is observed at all in isolated molecules. Any external perturbation is likely to further relax the selection rule. In liquid ketene, for example, the maximum absorbance intensity of the transition is enhanced by a factor of ~ 2 .⁴⁵ Although similar forces are responsible for condensation and physisorption, the latter must generally be greater in magnitude: adlayer formation is spontaneous below the bulk condensation pressure.

The signal below 230 nm corresponds to gas-phase excitation of the 1B_1 state. The maximum molecular cross section is 1.5 times greater in the adsorbed sample. Because the $^1B_1 \leftarrow ^1A_1$ transition is electric dipole allowed, there is less intensity to be gained by external perturbation of the molecule. Nevertheless, small distortions of molecular geometry can enhance the cross section of an allowed electronic transition. Vibrational distortion of isolated molecules⁵⁰ and surface-induced distortion of adsorbates⁵¹ can

(45) Laufer, A. H.; Keller, R. A. *J. Am. Chem. Soc.* **1971**, *93*, 61.

(46) Rabalais, J. W.; McDonald, J. M.; Scherr, V.; McGlynn, S. P. *Chem. Rev.* **1971**, *71*, 95.

(47) Price, W. C.; Teegan, J. P.; Walsh, A. D. *J. Chem. Soc.* **1951**, 920.

(48) Dixon, R. N.; Kirby, G. H. *Trans. Faraday Soc.* **1966**, *62*, 1406.

(49) Frueholz, R. P.; Flicker, W. M.; Kuppermann, A. *Chem. Phys. Lett.* **1976**, *38*, 57.

(50) Zittel, P. F.; Masturzo, D. E. *J. Chem. Phys.* **1986**, *85*, 4362.

(51) Swanson, J. R.; Friend, C. M.; Chabal, Y. J. *J. Chem. Phys.* **1987**, *87*, 5028.

(43) Yamaguchi, Y.; Frisch, M.; Gaw, J.; Schaefer III, H. F.; Binkley, J. S. *J. Chem. Phys.* **1986**, *84*, 2262.

(44) Penner, S. S. *Quantitative Molecular Spectroscopy and Gas Emission Spectroscopy*; Addison-Wesley: Reading, MA, 1959.

produce enhancements of the order observed here.

The signal near 265 nm has no analogue in the electronic spectrum of ketene gas. Therefore, we must assess the possibility of contamination. A fully allowed transition in a trace contaminant could produce absorbances that are comparable to the weak ketene signals. Such contaminants in the sample itself should have appeared in the 28-mbar gas spectrum. On the other hand, the contaminant may have been generated by reaction among adsorbed ketene molecules. Of the contaminants observed in the infrared spectrum, only diketene has an ultraviolet absorbance in this frequency range. In solution, the maximum absorbance of diketene occurs at a wavelength less than 250 nm.⁵² Furthermore, when the ketene on the film was intentionally converted to diketene, the gross features of Figure 5 were not intensified. The spectrum changed qualitatively. It is therefore unlikely that the 265-nm absorbance is due to diketene. We cannot rule out the possibility that it arises from a trace impurity, thermally generated and below the limit of infrared detection.

Another explanation for the 265-nm signal is suggested by Figure 9. Ketene has an electronic state between 1A_2 and 1B_1 ; 3A_1 . This state is not observed in gas-phase ultraviolet absorption studies because of the spin multiplicity selection rule. The level has been measured by electron impact energy loss spectroscopy, for which the transition is allowed. Also, triplet methylene (CH_2) is produced during mercury-sensitized dissociation of ketene, suggesting that collisions with 3P_1 mercury produce triplet ketene.⁵³ Since 3P_1 mercury is the source of 254-nm light, this is evidence that the 3A_1 state is energetically accessible near 265 nm.

Singlet-triplet transitions that are forbidden in the gas phase are sometimes observed in condensed systems—solutions, matrices, glasses—particularly in the presence of molecular oxygen.⁵⁴ This is generally attributed to the possibility of a charge-transfer complex in which oxygen accepts an electron. The singlet and triplet states are mixed in the complex; thus, the direct optical transition between them can borrow intensity from the complex-forming transition.⁵⁵ Studies of alkali-metal halide films by ultraviolet absorption and electron spin resonance have shown that they contain large numbers ($>3 \times 10^{18} \text{ cm}^{-3}$) of electronic defects such as F and V centers.^{39,56} When located at a surface, such defects are preferred adsorption sites; they can even act as catalysts.¹⁸ The spontaneous formation of charge-transfer complexes between defects and adsorbates had been observed directly: NO^+ and NO^- on LiF,³⁹ CO^+ on KCl.⁵⁶ It is possible, therefore, that the 265-nm signal is the $^3A_1 \leftarrow ^1A_1$ transition of ketene, enhanced by the presence of defects. This activity of alkali-metal halide films should be confirmed and explored with other molecules.

Photolysis of Adsorbed Ketene: Stoichiometry. The integrated infrared cross sections presented earlier can be used to quantify the photochemical reaction data. We integrate eq 4 over frequency and insert the window area A_w to give an expression for M , the number of molecules present:

$$M = N_{2D}A_w = 2.303\bar{A}/\bar{\sigma}_i \quad (5)$$

An infrared spectrum was recorded immediately before any ultraviolet irradiation and immediately after each of six successive exposures. Six bands were integrated in each spectrum: $CO_2 \nu_3$ and $C_2H_4 \nu_{12}$, from which the area before irradiation was subtracted; ketene ν_2 and CO, which were deconvoluted as described above; and ketene ν_3 and ν_4 . The band areas were then converted to M with the appropriate empirical or approximate $\bar{\sigma}_i$. This number of molecules is plotted as a function of ultraviolet exposure time in Figure 10. Three hours has been edited from the time scale; no data points were removed, and the lines connecting data

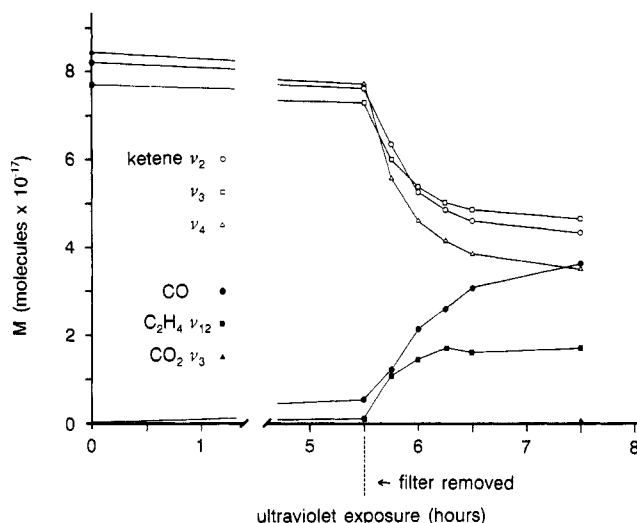
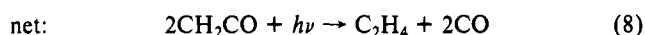
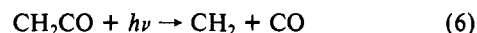


Figure 10. Photometric survey of ketene depletion and product accumulation during photolysis at 20 K. The number of molecules M was calculated from infrared absorbance band areas. During the initial 5.5-h exposure a glass filter which transmitted 254-nm light was used to prevent 185-nm light from entering the cell.

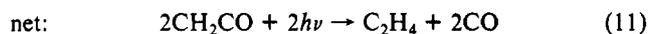
points across the break were drawn with the appropriate full-scale slope. The glass filter was in place for the first 5.5 h only. Ketene cross sections were measured during dosing at 150 K; the band areas changed slightly when the cell was cooled to 20 K. Therefore, the three ketene lines do not originate at a common point. The initial product amounts are zero by definition.

The quantity of ketene depleted over the entire exposure is 4.0×10^{17} molecules (an average of the ν_2 , ν_3 , and ν_4 measurements); this is 49% of the initial amount present. The amount of CO generated is 3.6×10^{17} molecules, or 90% of the ketene consumption. The amount of C_2H_4 produced is 1.7×10^{17} molecules; this is 43% of the ketene loss, or 47% of the CO generation. Only 1.1×10^{16} molecules of CO_2 are formed, or 2.7% of the ketene consumption.

Nascent methylene radicals that do not recombine with CO are likely to encounter unreacted ketene molecules



or other methylene radicals



The chemical stoichiometry of overall reactions 8 and 11 is the same and agrees with the reactant/product ratios observed. The mechanisms differ only in the quantum yield of products (or ketene consumption). Mechanism (6)–(8) predicts the loss of two ketene molecules per primary photochemical event. Mechanism (9)–(11) predicts unit efficiency. An empirical yield will be estimated in the following section, where we consider the dramatic increase in reaction rate when the filter is removed.

Another notable property of the ketene depletion curves is the subsequent decrease in reaction rate. Ketene consumed according to eq 9 or (assuming a steady-state concentration of CH_2) eqs 6 and 7 would exhibit first-order kinetics. The number of molecules is expected to decay exponentially with time to zero. As seen in Figure 10, ketene absorbance bands are only depleted to $\sim 50\%$ of their initial areas. Accumulation of CO in the film may be responsible. As photolysis proceeds the probability of $CO + CH_2$ recombination increases; therefore any first-order rate law is incomplete. Two further influences on the observed depletions deserve mention:

(52) Calvin, M.; Magel, T. T.; Hurd, C. D. *J. Am. Chem. Soc.* **1941**, *63*, 2174.

(53) Duncan, F. J.; Cveticovic, R. J. *J. Am. Chem. Soc.* **1962**, *84*, 3593.

(54) Becker, R. S. *Theory and Interpretation of Fluorescence and Phosphorescence*; John Wiley & Sons: New York, 1969.

(55) Tsubomura, H.; Mulliken, R. S. *J. Am. Chem. Soc.* **1960**, *82*, 5966.

(56) Zecchina, A.; Scarano, D. *Surf. Sci.* **1986**, *166*, 347.

First, ultraviolet light may not reach all portions of the film that are interrogated by the FTIR. If the window farthest from the lamp is not illuminated, then 50% depletion of infrared bands is to be expected. Ultraviolet absorption spectra show that the entire cell, with a typical annealed film present (but before addition of ketene), transmits at least 30% of light throughout the frequency range of interest. Since the ultraviolet irradiation geometry was designed to mimic the infrared beam, the far window should receive a significant fraction of the radiation that passes through the near one. This was confirmed by a simple test. An adsorbed ketene sample was exposed to unfiltered light until the reaction rate was nil. The ultraviolet lamp was then moved to the other side of the film cell, effectively reversing the near and far window positions. Further irradiation did *not* significantly increase the band loss rate; depletions remained near 50%. We also note unpublished results with a different molecule. Adsorbed hydrogen sulfide was photolyzed under conditions analogous to those described here. Depletion of S-H stretching band areas was limited to ~50%. Again, subsequent direct irradiation of the far window had no further effect.

Second, we consider an oversimplification which was made in the construction of Figure 10. The Beer-Lambert law describes samples of randomly oriented molecules. Thermal motion in a gas or liquid sample ensures isotropy. Although adsorbates on an individual NaCl(100) face may be highly ordered, the collection of crystallites that constitute a vapor-deposited film are randomly oriented. Therefore, the adsorbed sample as a whole is isotropic. Yet such samples have a novel feature: continuous thermal re-orientation can be frozen out. Consider now that a photochemical depletion process need not act isotropically. A beam of randomly polarized light has no component of electric field in the direction of propagation. It is preferentially absorbed by molecules whose active transition dipole has a large component normal to the direction of propagation. If a randomly oriented and locked sample is depleted by such a beam, the surviving molecules have a modified orientational distribution. Subsequent spectroscopic behavior is not described by the common Beer-Lambert law. It depends on the laboratory-frame relationship between depleting and interrogating beams, as well as the molecular-frame relationship between depleting and interrogating transitions. Therefore, the photometry of undepleted ketene is not straightforward. The conversion from infrared band area to number of molecules should incorporate explicitly the evolving orientational distribution. A formal treatment of these ideas will be the subject of a separate paper.

Photolysis of Adsorbed Ketene: Quantum Yield. For near-ultraviolet wavelengths below 313 nm isolated ketene molecules dissociate with unit quantum efficiency.³¹ The raw reaction rate of adsorbed ketene increases sharply when 185-nm light—instead of 254 nm—is allowed into the cell. Of course, this is due in part to the large cross section of the sample at 185 nm. Since the flux of ultraviolet photons through the sample is roughly known, an absolute quantum yield at each wavelength can be estimated from the empirical cross sections and reaction rates.

Quantum yield of dissociation, Φ , is a ratio of the molecular dissociation rate to the photon absorption rate. The former can be computed from slopes in Figure 10. The kinetic and photometric errors discussed earlier increase as depletion proceeds; *initial* dissociation rates are reflected in a pure and isotropic sample, thus containing minimal errors. It is assumed that the filtered output contains only 254-nm light. The next strongest mercury resonance line passed by the filter, 313 nm, is roughly 20 times less intense and overlaps a weaker absorbance in the sample.

The ketene consumption rate during the first 5.5 h of photolysis, r^{254} , is 3.0×10^{12} molecules s^{-1} (an average of the ν_2 , ν_3 , and ν_4 rates). The initial raw consumption rate with unfiltered radiation is 1.7×10^{14} molecules s^{-1} . To isolate the 185-nm contribution, recall that the filter's transmittance at 254 nm was 55%. The contribution by unfiltered 254-nm light is therefore $(3.0 \times 10^{12} s^{-1}/0.55)$. Subtracting this gives $r^{185} = 1.6 \times 10^{14} s^{-1}$.

We next need to estimate the rate, p , at which photons are absorbed by the adsorbed ketene. From the characteristics of the

photolysis lamp we calculate 2.9×10^{15} photons $cm^{-2} s^{-1}$ at 254 nm and 2.1×10^{14} photons $cm^{-2} s^{-1}$ at 185 nm. Here we ignore the reduced light levels at the window farther from the lamp; this is somewhat compensated by neglecting light collected by the mirror. Losses in the windows and filter attenuate 254-nm light intensity by a factor of 0.50 before it reaches the sample; 185-nm light is attenuated by 0.72 when passing through the two windows. At $\theta_r = 0.55$ the initial concentration of ketene on the windows must be $(5.0 \times 10^{19}$ molecules for $\theta_r = 1) \times (0.55) \times (0.032$ on windows) $\times (1/0.95$ $cm^2)$, or $N_{2D} = 9.2 \times 10^{17}$ molecules cm^{-2} . Using the 254-nm optical cross section from Figure 6, $\sigma_i^{254} = 4.7 \times 10^{-19}$ cm^2 molecule $^{-1}$, with eq 3 we find $p^{254} = 5.1 \times 10^{14} s^{-1}$; the rate of photons absorbed by the adsorbed ketene. At 185 nm the sample is effectively opaque. All photons that reach the inside of the cell are absorbed, so $p^{185} = 1.5 \times 10^{14} s^{-1}$.

The quantum yields are therefore $\Phi^{254} = r^{254}/p^{254} = 5.9 \times 10^{-3}$ and $\Phi^{185} = 1.1$. The latter value matches the proposed mechanism in which all ketene is consumed photochemically, eqs 9–11. The mechanism with secondary ketene consumption, eqs 6–8, predicts $\Phi = 2$. Since this probably falls within the error range of the present calculation, we cannot confidently assess the relative contributions of different secondary reactions. It is nevertheless clear that the *primary* yield of photodissociation at 185 nm is on the order of unity. The primary yield at 254 nm is at least 2 orders of magnitude lower.

How Does the Substrate Influence Photochemistry? That the dissociation efficiency varies in this energy range is a significant departure from the behavior of isolated molecules. At first, such activity in physisorbed systems comes as a surprise. The van der Waals interactions that bind adsorbates are feeble in comparison to the chemical bonds rearranged during ultraviolet photochemistry. Relatively small shifts in the infrared spectrum of ketene on NaCl are consistent with physisorption of the *ground* electronic state. In the ultraviolet spectrum, however, large changes in molecular cross section and absorption frequency imply a substantial perturbation of the *excited* electronic states. Molecular photochemistry may be influenced by both static and dynamic aspects of adsorbate/substrate interaction.

Deformation of an excited-state potential surface by the substrate is a static effect. Such interaction involves mixing of the electronic states of ketene with those of exposed ions, ion vacancies, or other defects. How these changes influence the ketene/NaCl system is not known.

The alteration of relaxation pathways from excited molecular states into the surface is a dynamic effect; we can describe these changes in somewhat greater detail. Measurements in the gas phase show that the dissociative lifetime of ketene decreases with increasing excitation energy; 0.3 ns has been reported for 313-nm light.³¹ Electronic-to-electronic energy-transfer events occur on a comparable time scale. Therefore, the greater yield at 185 nm may reflect a shorter dissociative lifetime and the decreased likelihood of electronic quenching by the substrate.

This explanation is complicated by current understanding of the dissociation dynamics of ketene. Measurements^{27,28,30,31,57} and calculations^{25,26,41} give the following picture. The minimum dissociation energy corresponds to a 371-nm photon. Near this threshold attention and contention have focused on a production of singlet vs triplet methylene. Significantly above threshold (wavelengths less than 313 nm) dissociation proceeds in two steps: the optically prepared state is in-plane bent $^1A''$, corresponding to 1A_2 excitation. It undergoes rapid internal conversion to the ground electronic state, which then has sufficient vibrational energy to dissociate. The next available excitation, to 3A_1 , does not correspond to a valid potential energy minimum—it crosses the 3A_2 state. These triplets can dissociate along bent paths (with small barriers) or perhaps cross to the ground electronic state. At even higher energy, *ab initio* studies have shown that the 1B_1 and 3B_1 states can dissociate monotonically along a C_{2v} path. This feature of their potential energy surfaces is unique among the excited states that have been investigated. This path could escape

quenching mechanisms that involve vibrationally hot intermediates.

In the frequency range for which NaCl is transparent, it is poorly coupled to the internal vibrations of adsorbed molecules. The fundamental vibration of adsorbed CO is at 2155 cm^{-1} ; its adsorbed-phase overtone fluorescence lifetime is $\sim 4\text{ ns}$.⁵⁸ A simple model of vibrational energy transfer to a homogeneous dielectric substrate agrees quantitatively with this measurement.⁵⁹ Moreover, this model shows that coupling to low-frequency modes (in the range for which NaCl is opaque) is strong, as expected. At 500 cm^{-1} , near the three skeletal bending fundamentals of ketene, adsorbate vibrational lifetimes of only $\sim 1\text{ ns}$ are predicted. Since the relevant electronic states of ketene are bent, transitory electronic excitation will deposit large amounts of energy into these modes. Vibrational relaxation may then be fast enough to compete with vibrationally mediated dissociation mechanisms. Indeed, the present study finds dissociation from the $^1\text{B}_1$ state of adsorbed ketene to be more efficient than dissociation from a distinct, lower energy state ($^3\text{A}_1$?) by at least 2 orders of magnitude. Whether the active quenching mechanisms are electronic or vibrational has yet to be determined.

It is appropriate to compare our work concerning ketene on NaCl with that of Leggett et al.,²⁴ who have studied OCS on LiF(100) single crystal. Transfer of electronic excitation from defects in LiF to adsorbed OCS has been suggested. The dissociation of an adsorbed sample by 222-nm light was 10^3 – 10^4 times more efficient than in the gas phase. This is considered to be greater than any reasonable enhancement of the *molecular* ultraviolet cross section. Color centers in the bulk crystal are believed to absorb radiation and then transfer it to adsorbed molecules by a fast electronic-to-electronic mechanism. Large-scale enhancements were not observed with other adsorbates. The present study of ketene on NaCl employs different methods and develops complementary photometric specifications. We assume that active radiation is absorbed by molecules and then show that molecular quantum yield is reduced in the adsorbed phase; if absorption by the substrate in fact accounts for some dissociation, the yield reduction must be even greater in magnitude. On the other hand, Leggett et al. assume unit molecular quantum yield and then show that the overall dissociation cross section is enhanced; if the quantum yield is in fact lower the cross section enhancement must be even greater in magnitude. These arguments independently document a quenching effect and an enhancement effect, yet neither argument rules out the possibility that both effects occur together. The ultraviolet absorption spectra of ketene on NaCl do suggest a novel mechanism for enhanced absorption: the coupling of molecular singlet and triplet states via color centers. This interaction is of course sensitive to the proximity of defects; therefore, it should be sensitive to coverage, substrate preparation, spacer layers, etc. Unlike the mechanisms favored by Leggett et al. in explaining their data, it intensifies an optical transition

in the adsorbed molecule itself. The cross section of gaseous ketene at 264 nm is so small that even a weak absorbance, as observed in the adsorbed phase, constitutes a $\sim 10^3$ times enhancement. Its absolute value is nevertheless 2 orders of magnitude smaller than reported for the enhanced dissociation of OCS on LiF.

Summary

The ketene molecule continues to be a rich target of experimental and theoretical investigation. When adsorbed to a sodium chloride film, its infrared spectrum resembles that of solid and matrix-isolated samples. The spectrum is heterogeneously broadened and complicated; the detailed origins of these effects are not known. Nevertheless, infrared band areas and coverage dependences are a sensitive clue to the extent and nature of photochemical depletion.

Three absorbances in the ultraviolet spectrum of adsorbed ketene differ significantly from the corresponding gas-phase spectrum. The dipole-allowed transition to $^1\text{B}_1$ is shifted to higher energy, and its maximum cross section is enhanced by a factor of 1.5. The dipole-forbidden transition to $^1\text{A}_2$ is more dramatically enhanced—a factor of 10 at its maximum. A third absorbance is tentatively identified with excitation to $^3\text{A}_1$, which in isolated molecules is strictly forbidden by conservation of spin multiplicity. By analogy to other enhanced singlet–triplet transitions, the charge-transfer activity of sodium chloride defects is offered as an explanation. These spectra allow quantification and comparison of photochemical depletion rates on a molecular basis.

The overall photochemical behavior of the adsorbed system differs from that of a matrix-isolated sample. Secondary reaction of methylene radicals is observed; therefore, the primary photochemical fragments are able to separate. This is in keeping with the microscopically porous structure of NaCl films: adsorbates are not “caged”, yet escaping fragments must strike other portions of the film. It follows that reactive species are most likely to be trapped when initial coverage is very low. Dissociation is also modified on the molecular scale. Whereas gas-phase dissociation proceeds with unit quantum efficiency, a significant quenching of 254-nm excitation relative to 185 nm is found for adsorbed ketene molecules. On the basis of gas-phase studies we speculate that the lower energy dissociation proceeds through a vibrationally hot intermediate, the skeletal modes of which are efficiently quenched by the NaCl substrate. Direct dissociation of the higher energy $^1\text{B}_1$ state is predicted on the basis of theoretical calculations.

These experiments indicate that a variety of novel physical mechanisms couple sodium chloride films to adsorbed molecules. These should be confirmed and explored with other adsorbates. Further study of ketene as a probe of energy flow and source of methylene radicals is also warranted.

Acknowledgment. The authors thank Tony Huff for his participation. This work was supported by the donors of the Petroleum Research Fund, administered by the American Chemical Society.

Registry No. NaCl, 7647-14-5; CO, 630-08-0; ketene, 463-51-4.

(58) Chang, H.-C.; Ewing, G. E. *Phys. Rev. Lett.* **1990**, *65*, 2125.

(59) Chang, H.-C.; Ewing, G. E. *J. Electron Spectrosc. Relat. Phenom.* **1990**, *54/55*, 39.